Optics Letters

Efficient narrowband terahertz generation in cryogenically cooled periodically poled lithium niobate

Sergio Carbajo,[1,2,3,*] Jan Schulte,[1,2] Xiaojun Wu,[1,3] Koustuban Ravi,[1,4] Damian N. Schimpf,[1,3] and Franz X. Kärtner[1,2,3,4,5]

[1]Center for Free-Electron Laser Science, DESY, Notkestraße 85, Hamburg 22607, Germany
[2]Department of Physics, University of Hamburg, Hamburg 22761, Germany
[3]The Hamburg Center for Ultrafast Imaging, Luruper Chaussee 149, Hamburg 22761, Germany
[4]Department of Electrical Engineering and Computer Science, and Research Laboratory of Electronics, Massachusetts Institute of Technology, 77 Massachusetts Avenue, Cambridge, Massachusetts 02139, USA
[5]e-mail: franz.kaertner@desy.de
*Corresponding author: scarbajo@stanford.edu

Received 14 October 2015; revised 16 November 2015; accepted 17 November 2015; posted 18 November 2015 (Doc. ID 251861); published 10 December 2015

We present an efficiency scaling study of optical rectification in cryogenically cooled periodically poled lithium niobate for the generation of narrowband terahertz radiation using ultrashort pulses. The results show an efficiency and brilliance increase compared to previous schemes of up to 2 orders of magnitude by exploring the optimal pump pulse format at around 800 nm, and reveal saturation mechanisms limiting the conversion efficiency. We achieve $>10^{-3}$ energy conversion efficiencies, μJ-level energies, and bandwidths <20 GHz at ~0.5 THz, thereby showing unprecedented spectral brightness in the 0.1–1 THz range relevant to terahertz science and technology.

OCIS codes: (190.7110) Ultrafast nonlinear optics; (140.3070) Infrared and far-infrared lasers.

http://dx.doi.org/10.1364/OL.40.005762

An increasingly wide variety of applications in fundamental sciences and advanced technologies makes use of coherent terahertz waves, mainly due to their ability to stimulate distinct structural dynamics and properties of matter, such as inter- and intramolecular excitations [1,2], ultrafast phase-changes [3], chirality switching [4], or molecular orientation and alignment [5], among others. Many of these applications demand the development of narrowband terahertz radiation sources because they can select, switch, or control processes in distinctly defined frequency bands. A well-established source for narrowband and tunable terahertz emission is the gyrotron, a device capable of delivering MW-level terahertz power in cw operation up to ~200 GHz. When pulsed, gyrotrons typically emit pulses as short as nanoseconds at Hz repetition rates, thereby restricting their use to slow or static processes. In the pursuit of accessing future novel ultrafast applications, such as time-resolved microscopy [6] or electron acceleration [7], the promise of generating efficient high-field, narrowband, tunable, and ultrafast terahertz radiation lies in laser-based techniques. Generation methods include optical parametric oscillation (OPO), difference frequency generation (DFG) with two distinct narrowband lasers, and optical rectification (OR) of a single broadband pulse (or intrapulse DFG) in periodically poled (PP) crystals. Previous DFG work has proven successful through different schemes in achieving optical-to-terahertz energy conversion efficiencies in the order of $\sim 10^{-5}$ [8,9]. OPOs have demonstrated slightly better conversion efficiencies [10], but cast doubt about their frequency and bandwidth tunability, with difficulty in reaching bandwidths narrower than a few hundreds of GHz in the lower terahertz frequency regime [11]. Recent work in seeded parametric generation in bulk lithium niobate has shown remarkable progress on wide-tuning-range terahertz generation with efficiencies up to 10^{-4} [12].

Alternatively, OR in PP crystals was also demonstrated to produce frequency and bandwidth tunable terahertz radiation [13–16]. Here, a broadband optical pulse is rectified by a quasi-phase matched (QPM) material with alternating sign of second-order susceptibility $\chi^{(2)}$ [17], which enhances conversion efficiency by achieving longer interaction lengths in collinear geometries. In this process, the down-converted central terahertz frequency (ν_0) is primarily determined by the domain period (Λ) and the angle of observation (Θ) (defined as the angle relative to the normal of the lateral surface), and to a lesser extent by temperature (T) tuning via temperature dependent index of refraction ($\partial n/\partial T$). That is, the second-order polarizability results in terahertz emission with forward ($\Theta = \pi/2$), backward ($\Theta = -\pi/2$), and perpendicular ($\Theta = 0$) components relative to the direction of the pump k-vector at a frequency given by

$$\nu_0 = \frac{c}{\Lambda |n_p - n_{\mathrm{THz}} \sin \Theta|}, \tag{1}$$

where c is the speed of light in vacuum, and n_p and n_{THz} are the group index of the pump and refractive index of the terahertz wave, respectively. The frequency ν_0 can be tuned via poling period and/or temperature tuning. The shape of the generated terahertz waveform is influenced by the domain structure of the PP crystal. The relative spectral bandwidth ($\Delta\nu_0/\nu_0$) decreases by increasing the number of domains (N) [15]. Previous experimental demonstrations of this technique used femtosecond pump pulses in periodically-poled lithium niobate (PPLN) [13] and lithium tantalate [15]. At higher frequencies, where terahertz absorption is strong, surface emission was proposed in order to shorten the terahertz travel path inside the material while maintaining its longitudinal length [14].

OR in PP crystals has the potential of producing high-energy terahertz pulses with narrow bandwidth. In this Letter, we demonstrate an efficiency increase of about 2 orders of magnitude compared with data from previous OR experiments in PP crystals reporting conversion efficiencies of 10^{-5} [13,15]. Here, the optimization strategy consists of the following: (i) reducing the terahertz absorption of lithium niobate by cryogenic cooling; (ii) optimizing the pump pulse bandwidth; and (iii) exploring the impact of crystal length on efficiency saturation. To reveal design strategies, we conduct systematic measurements of the extracted terahertz power, energy, and efficiency, as well as the temporal waveform and corresponding spectrum as a function of five characteristic parameters, namely, average intensity (I) [defined as the energy inside the crystal divided by the temporal pulse duration (Gaussian FWHM) and beam mode area (πw^2)], bandwidth ($\Delta\lambda$), geometric crystal length (L), domain period (Λ), and temperature (T).

As illustrated in Fig. 1, we employ compressed pulses from a Ti:sapphire laser amplifier. The system outputs mJ-level pulses at 1 kHz repetition rate at a wavelength of around 800 nm. A variable slit in the grating-pair compressor controls the bandwidth, ranging approximately between 3.5 and 10 nm. All QPM structures are made of 5 mol. %-doped congruent z-cut PPLN crystals. Each crystal is chromium-coated on all lateral surfaces and placed in a cryostat chamber pressure-connected to a LN_2 dewar. The temperature is measured using a silicon diode sensor glued to the crystal surface. At the PPLN input facet, the mode profile of the pump is 2.7 mm in diameter at $1/e^2$. The terahertz radiation exits the cryostat chamber through a 3.5 mm thick polymethylpentene (TPX) window. The chamber pressure level is lower than 10^{-5} mbar. The extracted radiation is collected and transported through two 90-deg off-axis parabolas with 2″ apertures and NA = 1 in a $4f$-configuration. At the terahertz image plane, the temporal waveform of the extracted terahertz spectrum is measured through electro-optic (EO) sampling in 0.5 mm-thick ZnTe using a small fraction of the pump beam as the EO probe. At the same image plane, albeit not depicted in Fig. 1, the extracted terahertz power is measured with both a pyroelectric detector (Gentec-EO Model THZ-B) and a calibrated thermal power sensor (Ophir-Spiricon Model 3A-P-THz). In the following, the reported efficiency is directly calculated from the measured power without compensating for Fresnel losses at the PPLN output facet (~45–48%) or transmission losses through the TPX outcoupling window (~18–22%). Note that a through-hole in the first collecting parabola serves as an outlet for the pump beam. The beam is then collected by an integrating sphere fiber-coupled to an optical spectrum analyzer to monitor the pump spectrum shaped by the inherent down-conversion of OR.

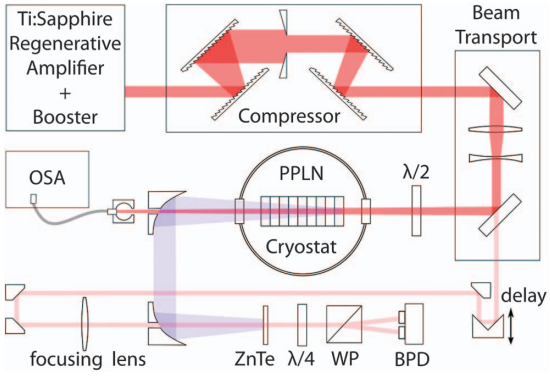

Fig. 1. Schematic of the experimental setup in EO-sampling configuration. OSA, optical spectrum analyzer; WP, Wollaston prism; BPD, balanced photodiode.

In the first set of measurements, we study the effect of crystal temperature. Cryogenic cooling is known to reduce the terahertz linear absorption of lithium niobate [15]. This reduction is relevant in QPM structures, since longer nonlinear interaction lengths may enhance conversion efficiency before absorption imposes limitations. As shown in Fig. 2(a), we measure a fivefold increase in extracted energy from the same PPLN crystal

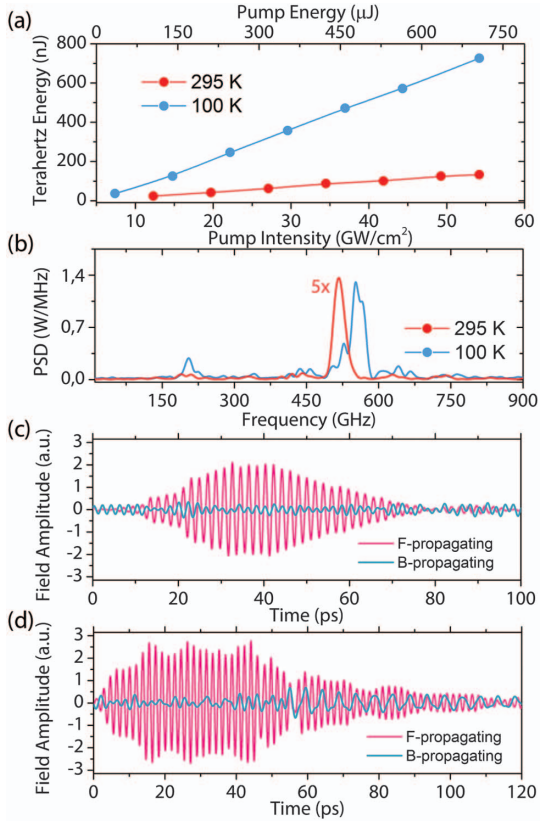

Fig. 2. Influence of temperature ($L = 5$ mm; $\Lambda = 212$ μm). (a) Terahertz energy as a function of pump energy and intensity; (b) PSD, corresponding power spectral densities with peak frequencies $\nu_0 = 520$ GHz ($T = 300$ K) (5× magnified) and $\nu_0 = 559.4$ GHz ($T = 100$ K); (c) and (d) forward- ($\nu > 375$ GHz) and backward-propagating ($\nu \leq 375$ GHz) decomposed temporal waveforms at 295 K and 100 K, respectively.

($L = 5$ mm and $\Lambda = 212$ μm) when reducing its temperature from 295 K to 100 K. In this data set, the PPLN is pumped with the full laser bandwidth of about 10 nm. The peak emission frequency corresponding to the 295 K spectrum [Fig. 2(b)] is 520 GHz, while at 100 K it shifts to 559.4 GHz, due to the change in refractive index with temperature. As shown in Fig. 2(b), the backward-propagating terahertz spectral components (i.e. counter-propagating w.r.t. the pump k-vector) emerge around 200 GHz, most notably at lower temperatures because of the reduced absorption. Figures 2(c) and 2(d) show the temporal waveforms retrieved by EO-sampling at 295 K and 100 K, respectively. The normalized temporal waveforms are color-overlaid in the forward- (magenta) and backward-propagating (blue) components with their relative field strengths. Higher terahertz absorption at room temperature severely weakens the EO-sampled backward-propagating wave [Fig. 2(c) in blue]. Conversely, at cryogenic temperatures [Fig. 2(d)], the back-propagating waves, which are detected simultaneously (Fig. 1), are again prominently visible at ~58 ps, a delay with respect to the forward-propagating wave that corresponds to the reflection of the backward-propagating wave at the entrance facet of the PPLN and then propagating over one entire crystal length before it exits its output facet.

The bandwidth of the pump has a strong effect on the amount of energy transferred into the fundamental QPM terahertz wave. Previous analytical studies have already shown efficiency tradeoffs between pump fluence and bandwidth [17], resulting in efficiencies peaking at about 4 nm bandwidth in the current range of parameters. For a given terahertz frequency (determined by Λ), the spectral bandwidth of the pump laser must support the right frequency spacing for down-conversion. For bandwidths smaller than the optimum, there are not enough

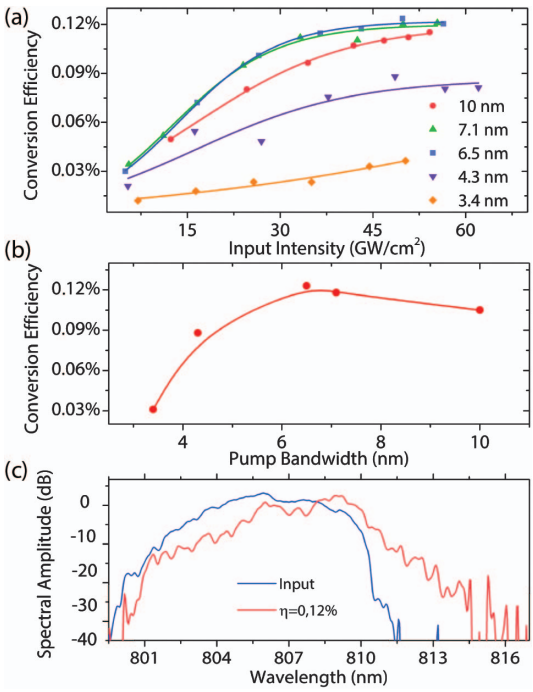

Fig. 3. Influence of pump pulse format ($L = 5$ mm; $\Lambda = 212$ μm; $T = 100$ K). (a) Extracted efficiency as a function of pump intensity for bandwidths ranging from 3.4 to 10 nm; (b) efficiency as a function of bandwidth for a pump intensity of 50 GW/cm^2; (c) recorded input and output optical spectra for highest achieved conversion efficiency (at $\Delta\lambda = 6.5$ nm and I = 50 GW/cm^2).

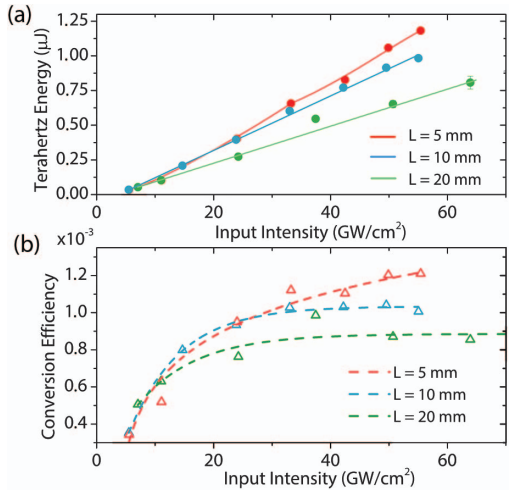

Fig. 4. (a) Terahertz energy and (b) conversion efficiency ($T = 100$ K; $\Lambda = 212$ μm; $\Delta\lambda = 6.5$ nm) for $L = 5$, 10, and 20 mm. Peak emission is ~520 GHz for all three crystal lengths. Solid and dashed splines are visual guidelines.

photon pairs at the right frequency spacing. For bandwidths larger than the optimum, dephasing effects take place as well as energy transfer into odd harmonics of the fundamental terahertz wave due to high grating harmonics of the poling. We investigate the efficiency (η) extracted from the same PPLN crystal ($L = 5$ mm; $\Lambda = 212$ μm; $T = 100$ K) at around 500 GHz as a function of the bandwidth of the 800 nm pump pulse. Figure 3(a) shows the energy efficiency curves corresponding to different pump bandwidth as a function of pump intensity. These results are depicted in Fig. 3(b) for a fixed intensity of 50 GW/cm^2. A maximum energy conversion efficiency of 0.12% is achieved at around 6.5 nm. The increase in optical-to-terahertz energy transfer is also observed in the red-shifted pump spectrum [Fig. 3(c)]. This few-nm red-shift arises from cascaded down-conversion of optical photons, which undergoes more cascaded cycles as the process becomes more efficient.

At cryogenic temperatures, the terahertz absorption coefficient at around 0.5 THz is sufficiently small (as shown in Fig. 2) that the conversion efficiency benefits from longer crystal lengths (L). Longer L with same Λ ($L = N\Lambda$) would also yield emission with narrower linewidth, since $\Delta\nu \propto N^{-1}$. However, it is expected that the interplay between the pump intensity I and L may limit the down-conversion process. For instance, self-focusing and self-phase modulation may act upon the spatiotemporal phase of the pump pulse at sufficiently high

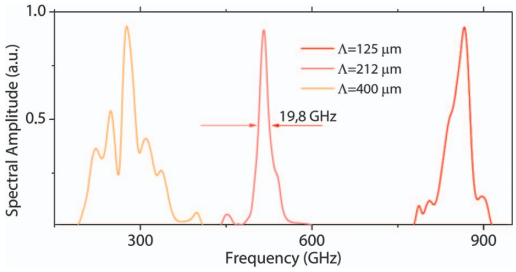

Fig. 5. Spectral amplitude of 10 mm crystals ($T = 295$ K). The peak frequencies are $\nu_0 = 276$, 513, and 867 GHz, for the domain periods 400, 212, and 125 μm, respectively.

Table 1. Summary of Operational System Specifications at Cryogenic and Room Temperature

QPM Crystals			Optical Pump			Terahertz Waves					
						ν_0 [GHz]		$\Delta\nu$ [GHz]		η [$\times 10^{-3}$]	
Λ [μm]	L [mm]	N	$\Delta\lambda$ [nm]	t [fs][a]	I [GW/cm^2]	295 K	100 K	295 K	100 K	295 K	100 K
400	10	25	6–7	190–160	50–60	275.8	–	95.6	–	0.28	–
212	5	24				520.0	559.4	27.7	31.4	0.36	1.20
	10	48				517.5	561.8	19	18.6	0.19	1.03
	20	94				–	559.8	–	11.2	0.04	0.89
125	10	80				867.3	–	35	–	0.12	–

[a]Pulse duration measured with interferometric autocorrelator.

intensities. The roles of these and other mechanisms need further investigation.

In order to investigate the effect of crystal length, we measure the terahertz energy and efficiency with respect to pump intensity for three different crystal lengths ($L = 5$, 10, 20 mm) and same domain period ($\Lambda = 212$ μm) at 100 K. As shown in Fig. 4(a), the terahertz energy increases monotonically with pump intensity for all three L values. The 20 mm PPLN shows saturation of the conversion efficiency [Fig. 4(b)], which is more pronounced compared with the two other PPLNs. The scaling trend of the efficiency curve is best for the 5 mm crystal, and begins to roll off at intensities of about 30 GW/cm^2. Note that in this regime the photogenerated carrier concentration—which can severely absorb terahertz radiation—due to three photon absorption in lithium niobate is negligibly small [18]. Also, the pump power is 2 orders of magnitude above the critical power for self-focusing of about 10 MW, and there should be significant self-phase modulation due to large B-integral values. These nonlinear effects deteriorate the quality of the pump towards the end of the crystal (not shown). This may limit efficiency scaling using longer crystals due to a deteriorated pump where terahertz waves propagate with nonnegligible absorption. Such effects unfold in the measured temporal waveforms (Fig. 2). At room temperature, the trailing part of the waveform—which is generated first in the process—decays as expected, due to linear absorption in the PPLN. Without spatiotemporal beam distortions, the leading part of the waveform ought to reach the highest field amplitude, since it is generated last. However, the measurements show that the field amplitude also decays at the leading edge at cryogenic temperatures [Fig. 2(d)]. The amplitude decay at the leading part of the waveform confirms that the down-conversion process becomes inefficient towards the end of the crystal due to distortions of the pump beam.

Exploiting the low absorption coefficient of lithium niobate at cryogenic temperatures and optimizing the pump bandwidth permits terahertz generation with η of 10^{-4} to 10^{-3}, ν_0 in the 0.1–1 THz range and $\Delta\nu$ from 10 to 100 GHz. Figure 5 exemplifies this capability with spectra acquired employing 10 mm-long PPLNs with different poling periods. Table 1 provides a more complete overview of measured parameters for different L and Λ. There the terahertz linewidths are the FWHM values of Lorentzian line-shape fits of the spectral amplitude.

In conclusion, we have scaled the conversion efficiency of narrowband terahertz generation in PPLN to above 10^{-3} in the sub-THz frequency range. These results were achieved by rectifying high peak-power ultrashort pulses. At frequencies of around 0.5 THz, pumping of cryogenically cooled PPLN crystals with optimized spectral bandwidth (6–7 nm for 800 nm pulses) resulted in 0.12% efficiency and more than 1 μJ of terahertz pulse energy. Based on the current experiment and crystals used, it appears that extending the crystal length beyond 10 mm is disadvantageous for efficiency scaling due to limitations imposed by the combination of terahertz absorption and spatial-temporal distortions of the pump. Detailed causes of such distortions are subject of ongoing research.

Funding. European Research Council (ERC) (FP/2007-2013).

Acknowledgment. We thank Oliver Mücke, Giovanni Cirmi, and Giulio Rossi for their support with the laser source.

REFERENCES

1. M. van Exter, C. Fattinger, and D. Grischkowsky, Opt. Lett. **14**, 1128 (1989).
2. M. Walther, P. Plochocka, B. Fischer, H. Helm, and P. Uhd Jepsen, Biopolymers **67**, 310 (2002).
3. M. Liu, H. Y. Hwang, H. Tao, A. C. Strikwerda, K. Fan, G. R. Keiser, A. J. Sternbach, K. G. West, S. Kittiwatanakul, J. Lu, S. A. Wolf, F. G. Omenetto, X. Zhang, K. A. Nelson, and R. D. Averitt, Nature **487**, 345 (2012).
4. S. Zhang, J. Zhou, Y.-S. Park, J. Rho, R. Singh, S. Nam, A. K. Azad, H.-T. Chen, X. Yin, A. J. Taylor, and X. Zhang, Nat. Commun. **3**, 942 (2012).
5. S. Fleischer, Y. Zhou, R. W. Field, and K. A. Nelson, Phys. Rev. Lett. **107**, 163603 (2011).
6. T. L. Cocker, V. Jelic, M. Gupta, S. J. Molesky, A. J. Burgess Jacob, G. D. L. Reyes, L. V. Titova, Y. Y. Tsui, M. R. Freeman, and F. A. Hegmann, Nat. Photonics **7**, 620 (2013).
7. L. J. Wong, A. Fallahi, and F. X. Kärtner, Opt. Express **21**, 9792 (2013).
8. W. Shi and Y. J. Ding, Appl. Phys. Lett. **83**, 848 (2003).
9. K. Miyamoto, H. Minamide, M. Fujiwara, H. Hashimoto, and H. Ito, Opt. Lett. **33**, 252 (2008).
10. T. Taniuchi, S. Okada, and H. Nakanishi, J. Appl. Phys. (Melville, NY, U.S.) **95**, 5984 (2004).
11. J. E. Schaar, K. L. Vodopyanov, and M. M. Fejer, Opt. Lett. **32**, 1284 (2007).
12. S. I. Hayashi, K. Nawata, T. Taira, J.-I. Shikata, K. Kawase, and H. Minamide, Sci. Rep. **4**, 5045 (2014).
13. Y.-S. Lee, T. Meade, V. Perlin, H. Winful, T. B. Norris, and A. Galvanauskas, Appl. Phys. Lett. **76**, 2505 (2000).
14. C. Weiss, G. Torosyan, Y. Avetisyan, and R. Beigang, Opt. Lett. **26**, 563 (2001).
15. L. Palfalvi, J. Hebling, J. Kuhl, A. Peter, and K. Polgar, J. Appl. Phys. **97**, 123505 (2005).
16. K. L. Vodopyanov, X. Yu, J. S. Harris, Y.-S. Lee, W. C. Huribut, V. G. Kozlov, D. Bliss, and C. Lynch, Appl. Phys. Lett. **89**, 141119 (2006).
17. K. L. Vodopyanov, Opt. Express **14**, 2263 (2006).
18. B. S. Wherrett, J. Opt. Soc. Am. B **1**, 67 (1984).